The claustrum of the pig: an immunohistochemical and a quantitative Golgi study

Andrea Pirone [1], Vincenzo Miragliotta[1], Bruno Cozzi[2], Alberto Granato[3]

1 Department of Veterinary Sciences, University of Pisa, Pisa, Italy

2 Department of Comparative Biomedicine and Food Science, University of Padova, Legnaro (PD), Italy

3 Department of Psychology, Catholic University of the Sacred Heart, Largo A. Gemelli 1, 20123 Milan, MI, Italy

Correspondence:

Andrea Pirone

andrea.pirone@unipi.it

Running title: The claustrum of the pig

ABSTRACT

The brain of the pig, due to its similarities with the cortical and subcortical structures of the human brain, is considered an interesting model for neurochemical studies. In addition, it presents a peculiar morphology of the claustrum (Cl) characterized by a wide posterior enlargement, an ideal structure for physiological investigations. Despite increasing interest in the Cl over the last decades its function is still a puzzling problem. There is a wealth of data on general anatomy, cytoarchitecture, and chemoarchitecture but much less is known about the dendritic morphometry of the claustrum neurons. Dendritic length and branching pattern are key features to understand the microcircuitry organization and thus the delineation of the structure-function relationships of the Cl. In the attempt to better understand the morphology and the circuitry of the claustrum, we undertook a quantitative study of the dendrites of the spiny neurons employing the Golgi staining and an immunohistochemical analysis to describe the distribution of the parvalbumin (PV)-immunoreactive interneurons throughout the pig claustrum. Taken together, the results described herein showed that the different distribution of the PV expressing interneurons and the different dendritic architecture corresponded to the change of the pig claustrum shape in its rostro-caudal axis suggesting for the large posterior puddle a unique function.

Key words: claustrum, dendrite, parvalbumin, pig, Golgi staining

INTRODUCTION

The claustrum is a ribbon-like structure of gray matter located in the ventrolateral telencephalon of all the mammals examined so far, including man (Kowianski et al. 1999). Its function, structural organization, and origin are still a matter of debate (Edelstein & Denaro, 2004; Crick & Koch, 2005; Pirone et al. 2012; Mathur, 2014; Deutch & Mathur, 2015; Goll et al. 2015). The extensive links of the Cl with different cortical, subcortical structure and afferents from the brainstem have been described recently (Day-Brown et al. 2016; Reser et al. 2017; Wang et al. 2017; Pirone et al., 2018; White & Mathur, 2018). However, despite the wealth of data on general anatomy, cytoarchitecture, and chemoarchitecture (Rahman & Baizer, 2007; Kowianski et al. 2009; Cozzi et al. 2014; Hinova-Palova et al. 2014; Pirone et al. 2014, 2015, 2016; Orman et al. 2016) much less is known about the dendritic morphometry of the claustrum neurons. The Golgi staining or "la reazione nera" (the black reaction) discovered by Camillo Golgi in 1873 is one of the best and most elegant methods to observe the morphology of the whole neuron; it still represents the standard for visualization of dendrites and spines, even if only about 1-10% of neurons are stained (Shankaranarayana et al., 2004). Golgi or Golgi-like methods have been used to study the normal and abnormal neuronal morphology in different animals (Jacobs et al., 2001; Giannetti et al. 2000; Di Rocco et al. 2002, 2001; Granato et al. 2003; Anderson et al. 2009; Butti et al. 2015; Johnson et al. 2016; Bicanic et al. 2017). Use of the Golgi staining identified different types of neurons in the claustrum of cat, monkey and human (Brand 1981; LeVay & Sherk 1981; Braak & Braak 1982) but little is known about the dendritic architecture. Dendritic length and branching pattern are key feature to understand the microcircuitry organization (Hamilton et al., 2012; Rees et al., 2017) and thus the delineation of the relationship between structure and function relationships of the Cl.

PV is a calcium binding protein expressed by fast-spiking inhibitory interneurons involved in the generation of network oscillation and able to shape complex network functions (Hu et al. 2014). A recent study demonstrated the role of the PV interneurons in the modulation of the activity of the claustro-cortical neurons (Kim et al. 2016).

The pig is considered an interesting model for biomedical research. The swine brain is closer than the rat to some of the anatomical and functional characteristics of the primate brain. Because of that, the number of studies employing the pig brain as a model for neurochemical studies has increased dramatically over the past decades (Jelsing et al. 2006; Lind et al.2007). In particular the Cl of the pig is characterized by a wide enlargement called "puddle" suited for physiological recording, differently from other species in which the small size of the nucleus and its continuity with adjoining structures are particularly challenging for recording (Johnson et al. 2014). Here, in an attempt to better

understand the morphology of this nucleus, we undertook a quantitative study of the dendrites of its spiny neurons, employing the Golgi staining and the Neurolucida software. Furthermore, by immunohistochemical analysis we tried to describe the distribution of the PV-immunoreactive (ir) neurons throughout the pig claustrum.

MATERIALS AND METHODS

Animals and tissue sampling

The brains of 5 females (*Sus scrofa domesticus*) 9 months old of 165-170 Kg body weight were removed immediately after commercial slaughtering at a local abattoir (Desideri Luciano SPA, Via Abruzzi, 2 56025 - Pontedera PI, Toscana - Italy). Animals were treated according to the European Regulation (CE1099/2009) concerning animal welfare during the commercial slaughtering process and were constantly monitored under mandatory official veterinary medical care. All the animals were in good body condition and considered free of pathologies by the veterinary medical officer responsible for the health and hygiene of the slaughterhouse. The brains, extracted within 10 min of death, were cut into transverse sections (0.5 cm thick) containing the Cl and the adjoining structures (putamen and insular cortex) in their rostro-caudal extent. Tissue blocks of the right hemisphere were fixed overnight by immersion in 4% paraformaldehyde in 0.1 M phosphate-buffered saline (PBS) at pH 7.4 and routinely processed for paraffin wax embedding.

Three coronal tissue blocks of each brain were chosen following three levels: rostral, middle and caudal. The levels and the boundaries of the claustrum were identified according to a stereotaxic atlas (Félix et al., 1999) using these coordinates: rostral, A 17.50; middle, A 5.00; caudal, A 0.50.

Golgi-Cox staining

Tissue Blocks of the left hemisphere were processed for Golgi-Cox staining according to the method reported by Zaqout and Kaindal (2016). Briefly, tissue blocks were quickly washed with double distilled water (dd-H2O) and transferred into the Golgi-Cox solution at room temperature in the dark for 10 days. Each block was then washed with dd-H2O, put into tissue-protectant solution and stored at 4 °C in dark for 7 days. The samples were then embedded in 4% low melting agarose and subsequently sectioned with a vibratome (Leica VT1200S). 200 µm thick-sections were collected onto gelatin-coated slides and kept for drying in dark for 2-3 days. Finally, slides were developed, dehydrated with ethanol, cleaned with xylol and mounted with mounting media (DPX, WWR Internetional Ltd., Poole, England)

Neuron selection and quantification

Three relatively isolated neurons of the claustrum *per* tissue block (i.e., 9 cells *per* specimen) were chosen for analysis following these criteria: selected neurons had an isolated soma near the center of the 200 µm section with fully impregnated, relatively unobscured, and complete dendritic arborization.

Neurons were observed using a Nikon Eclipse E600 light microscope and traced under a planachromatic 40x objective along the x-, y-, z-coordinates using the Neurolucida software (MBF Bioscience, Inc., Williston, VT, USA).

Somata were traced first at their widest point in the two-dimensional plane to provide an estimate of their cross-sectional area. Subsequently, dendrites were traced somatofugally in their entirety. Dendritic arborizations were not followed into adjacent sections. Broken ends or ambiguous terminations were identified as incomplete endings and their parent dendrites excluded from the quantitative evaluation. A total of 45 neurons were traced by selecting all those that met the inclusion criteria set out above. For the completely reconstructed dendrites (n = 198) the following quantitative parameters were evaluated (see Fig. 3): a) total length of each dendrite (sum of the length of the primary dendrite originating from the soma and of all its daughter branches); b) number of terminal tips of each dendrite; c) terminal length percentage of each dendrite, i.e. the percentage of the total length occupied by the terminal branches.

Statistical analysis

Data regarding the three rostro-caudal levels of the claustrum are expressed as mean ± standard error of the mean. Differences among the different levels were evaluated using the ANOVA, followed by a post hoc test (Tukey HSD).

Immunohistochemistry

Immunoperoxidase reaction was performed on serial paraffin sections (5 µm) of the right hemisphere using a mouse monoclonal Anti-PV (1:2000, Sigma, P3088, Clone PARV-19) and a mouse monoclonal anti-NeuN (1:1000, Chemicon Int., MAB377, Clone A60) as neuronal marker. Epitope retrieval was carried out at 120 °C in a pressure cooker for 5 min with a Tris/EDTA buffer, pH 9.0. Sections were pretreated with 1% H_2O_2 (in 0.1 M phosphate-buffered saline (PBS), pH 7.4, 10 min) to quench endogenous peroxidase activity, then rinsed with 0.05% Triton-X (TX) -100 (in 0.1 M PBS, 3 x10 min), and blocked for 1 h with 5% normal horse serum (PK-7200, Vector Labs, Burlingame, CA) (in 0.1 M PBS). Serial sections were incubated overnight at 4 °C in a solution containing the anti-PV or the anti-NeuN with 2% normal horse serum, 0.05% TX-100 (in 0.1 M PBS). Sections were then rinsed in 0.1 M PBS, (3 x10 min), followed by incubation with biotinylated anti-mouse IgG (5 µg/ml, BA-2001, Vector Labs, Burlingame, CA) and then with ABC reagent (Vectastain Kit, PK-7200, Vector Labs, Burlingame, CA). Sections were again rinsed in 0.1 M PBS, for 3 x 10 min. Staining was visualized by incubating the sections in diaminobenzidine (sk-4105, Vector Labs) solution. The specificity of immunohistochemical staining was tested by replacing either the primary antibodies, anti-mouse IgG, or the ABC complex with PBS or non-immune serum. Under these conditions, staining was abolished. Purified frog muscle parvalbumin was used as the immunogen, the antibody reacts with PV (12 kDa) originating from human, bovine, goat, pig, rabbit, dog, cat, rat, frog and fish (manufacturer's technical information). Furthermore, specificity of the antibodies had already been tested in previous studies:

PV (http://antibodyregistry.org/AB_477329)

NeuN (http://antibodyregistry.org/AB_2298772)

RESULTS

Overview

In the series of rostral coronal blocks, the claustrum of the pig was located in the ventrolateral telencephalon and showed the classic ribbon-like shape (Fig. 1a). The nucleus then assumed a triangular aspect in the middle region (Fig. 1d). Interestingly, the caudalmost region of the claustrum was characterized by a large puddle (Fig. 1g). The immunoistochemical staining employing the NeuN as neuronal marker confirmed and well outlined the change of the claustrum shape in its rostrocaudal extent (Fig. 6a-8a).

Golgi-Cox staining

Photomicrographs of selected Golgi preparations indicate the overall high quality of the stain (Fig. 1). The claustrum was well impregnated (Fig.1 b, e, h) and its neurons with soma of different shape could be easily recognized (Fig. 1 c, f, i). An examination under higher magnification revealed that spiny neurons were the most common neuronal types impregnated in the claustrum (Fig. 2).

The quantitative parameters of claustral dendrites are shown in figure 3, 4 and 5. There was a significant difference for the terminal length percentage (TLP) across the three levels ($F_{2, 195} = 4.03$; $P < 0.05$). In particular, TLP was significantly lower for caudal sample than for the rostral and middle samples (Fig. 3C). The Sholl analysis confirmed that a substantial percentage of branching nodes in the caudal part of the claustrum occurs at a considerable distance from the soma (Figure 5). The length and the number of terminal tips did not reveal significant differences among the three levels.

NeuN

In the rostral coronal paraffin sections, the NeuN labeling depicted the Cl of the pig as a band-like structure extending dorsoventrally along the adjacent cortex (Fig. 6a). Caudally, we found a level where NeuN immunostaining showed the change of shape of the claustrum. In particular, along with the strip-like shape the Cl began to expand in a pyramidal/triangular structure (Fig. 7a) which in the most caudal sections formed a large mass of grey matter called the posterior puddle (Fig. 8a).

Parvalbumin

The immunoperoxidase reaction on the paraffin sections revealed the absence of PV in the rostral part of the claustrum and in the adjacent cortex (Fig. 6 b, e, f). On the contrary, in the same sections PV-ir neurons were evident in the dorsal cortex (inset of Fig. 6 b). In the middle level very scanty positive neurons were only observed where the claustrum began to expand in a triangular structure (Fig. 7, b, c, d) while PV-ir neurons were still present in the dorsal cortex (inset of Fig. 7b). In the caudalmost sections, the large puddle of the claustrum presented numerous PV labeled neurons (Fig. 8 b, c, d).

DISCUSSION

In the present study we provide a quantitative analysis of the dendrites of the spiny neurons and the immunodistribution of the PV-positive neurons in the pig claustrum. In our Golgi stained samples, we focused on the spiny neurons because they represent the principal cells within the claustrum, that project to, and receive from, different cortical and subcortical areas (Brand 1981; LeVay and Sherk 1981; Braak and Braak 1982; Kim et al., 2016).

Golgi staining

Former studies employing the Golgi method are limited to a morphological description of the different types of the claustral neurons (Brand 1981; LeVay and Sherk 1981; Braak and Braak 1982). Here, we have quantitatively analyzed dendritic morphology of intraclaustral neurons in three consecutive rostro-caudal levels: rostral, middle and caudal. To our knowledge, this is the first report on the quantitative characterization of the dendritic branching in the mammalian claustrum.

Our data emphasize some differences of dendritic geometry along the rostro-caudal axis of the nucleus in the swine. The regional variability of dendritic architecture has been classically described in the neocortex, where pyramidal neurons of the high integration areas have longer and more branched dendrites than neurons in the motor, sensory or visual cortex (Elston et al., 2001; Jacobs et al., 2001; Jacobs et al., 2011; Butti et al., 2015; Jacobs et al., 2015; Johnson et al., 2016).

In particular, the percentage of dendritic length occupied by terminal branches (TLP) shows a regional dendritic variation throughout the pig claustrum: TLP was lower in the caudal level when compared to the rostral and middle sections. Both the TLP and the Sholl analysis thus suggest that caudal neurons display dendrites with branching points further from the soma, in comparison to more rostral neurons.

It is possible that some of the differences observed in the topological and metric properties of dendrites represents the consequence of geometric constraints owing to the different shape of the claustrum along its rostro-caudal axis. Nevertheless, these differences are likely to result in functional peculiarities of different claustral subdivisions. It is well known that the firing properties of neurons are determined not only by the distribution of ion channels, but also by the dendritic geometry (see, for instance, Mainen & Sejnowski, 1996; van Ooyen et al., 2002; Saparov and Schwemmer, 2015). Furthermore, while it is unlikely that claustrocortical neurons located in different claustral sectors are connected to each other (Kim et al., 2016), we cannot rule out that the longest dendritic trees of some neurons can provide a cross-talk between different functional zones (e.g., visual and auditory).

However, the TLP observed in our study for all the rostro-caudal levels is lower than that observed in neocortical pyramidal neurons of rodents (about 78% for rostral/middle levels, about 72% for

caudal levels; about 84% for neocortical neurons; see Granato et al., 2003). This may suggest that, although neocortex and claustrum share several neurochemical features (Pirone et al., 2012), claustral and cortical neurons perform different types of dendritic computation.

Immunohistochemistry

The data reported here show that the swine claustrum does not maintain the classical shape of other mammals in rostro-caudal direction. There is an ongoing debate on whether the endopiriform nucleus (En) is functionally and anatomically separate from the claustrum (Watson and Puelles, 2017). In our sections immunostained with NeuN we were not able to identify the En which was not reported in the stereotaxic atlas we referred to (Félix et al., 1999). However, we cannot exclude its presence considering that it has been described in different species (marmoset: Watakabe, 2017; rat: Watson et al., 2017; bat: Orman et al., 2017).

The NeuN labeling identified a peculiar enlargement in the caudalmost region, as previously described in a former study (Johnson et al., 2014).The PV-ir neurons not observed in the rostral sections were localized in this latter part. This particular pattern was not reported in other species, in which PV-ir neurons were seen throughout the claustrum (rat: Druga et al., 1993; monkey: Reynhout & Baizer, 1999; cat: Hinova-Palova et al., 2007; Rahman and Baizer, 2007; human: Hinova-Palova et al., 2014; human, chimpanzee, macaque: Pirone et al., 2014; dog: Pirone et al., 2015). The claustrum of the bottlenose dolphin contains no PV-positive neurons, a situation possibly related to the paucity of PV-ir neurons in the visual cortex of the same species (Cozzi et al., 2014). The link between these two areas has been clearly demonstrated in the cat. In fact, the postero-dorsal zone of the cat nucleus is called the visual claustrum, due to its connections with the visual cortex (LeVay & Sherk, 1981). Moreover, PV-ir neurons are observed in the cat visual claustrum (Rahman & Baizer, 2007). Interestingly, the visual claustrum of the macaque monkey (Baizer et al., 1993, 1997) is also located in the enlarged region. However, the latter part of the claustrum of the macaque is ventral, with a topography different from that of the cat and pig.

Neurons expressing PV are classically considered GABA-ergic interneurons mainly localized in the neocortex and in the hippocampus (see Hu et al., 2014 for review) even if PV is also reported in projection neurons of the substantia nigra (Gerfen et al., 1985), and trigeminal nucleus (Bennet-Clarke et al., 1992), and in thalamic neurons that project to the cortex (Rausell et al., 1992).

Nevertheless, PV immunohistochemistry has been proposed as a reliable and easy method to identify the nucleus (Mathur et al., 2009; Mathur, 2014). Our data obtained in the pig agree well enough with what reported for other mammals, but only if we consider the posterior puddle of the species. A recent, technically innovative study on the cellular organization of claustral circuits in the mouse

reported that intraclaustral PV-ir interneurons are highly interconnected and linked with the claustro-cortical neurons (Kim et al., 2016; White et al., 2018). In line with these researches, and with data reported in the visual cortex (Atallah et al., 2012), our results provide anatomical support to hypothesize a possible role of the PV-positive neurons of the large posterior claustrum in the modulation of the responses of the claustro-cortical neurons to visual stimuli. To this effect, it would be interesting to estabilish (e,g: performing a glutamic acid decarboxylase/PV co-localization) if the PV-positive cells of the pig claustrum are GABA-ergic interneurons.

The pig belongs to the Order Cetartiodactyla, in which, according to previous studies (Hof et al., 1999, 2000), PV is the least expressed of the three calcium binding proteins (CBP) while calretinin (CR) and calbindin (CB) are predominant in the neocortex. Furthermore, PV is not expressed in the claustrum of the bottlenose dolphin, a marine Cetartiodactyla (Cozzi et al., 2014), even the auditory and visual cortex of the same species (Glezer et al., 1995, 1998) and other cetaceans (Glezer et al., 1993) contain few PV-ir neurons, except in the zone comprised between layers IIIc/V and VI. A series of studies (Hof et al., 1999; Cozzi et al., 2017) established that the lamination of the neocortex in hoofed mammals consistently shows specific features that differentiate its organization (and potentially its circuitry) from that of primates, namely *a*) the expansion of layer I and II; *b*) the virtual disappearance of layer IV; and *c*) a certain difficulty to distinguish between layers V and VI.

Evidently, the lack of a definite layer IV in the neocortex of Cetartiodactyla (Hof et al., 1999; van Kann et al., 2017) and Perissodactyla (Hof et al., 1999; Cozzi et al., 2017) is related to the scarcity or absence of the typical thalamo-recipient granules, and consequently leads to a reduced expression of PV. Here we also emphasize that the organization of the thalamo-cortical projections in a five-layered cortex relies heavily on layers II and III (Godlove et al., 2014; Beul and Hilgetag, 2015), a feature that in hoofed mammals may be possibly connected to a fast response to stimuli required by the complexity of quadrupedal locomotion. How this feature may affect the reciprocal connections with the claustrum cannot be defined here. However, it would be important and interesting to ascertain whether the key features displayed by the claustrum of the pig are common also to other hoofed mammals.

Although we are aware of the limitations of the Golgi staining, the results described herein showed that the change of the pig claustrum shape in its rostro-caudal axis corresponds to a different distribution of the PV expressing neurons and to a different dendritic architecture suggesting for the large posterior puddle not only a morphological peculiarity but also a functional peculiarity.

REFERENCES

Atallah BV, Bruns W, Carandini M, Scanziani M. 2012. Parvalbumin-Expressing Interneurons Linearly Transform Cortical Responses to Visual Stimuli. Neuron 73:159–170

Baizer JS, Desimone R, Ungerleider LG. 1993. Comparison of subcortical connections of inferior temporal and posterior parietal cortex in monkeys. Visual Neurosci 10:59–72.

Baizer JS, Lock TM, Youakim M.1997. Projections from the claustrum to the prelunate gyrus in the monkey. Exp Brain Res 113:564–568.

Bennett-Clarke CA, Chiaia NL, Jacquin MF, Rhoades RW. 1992. Parvalbumin and calbindin immunocytochemistry reveal functionally distinct cell groups and vibrissa-related patterns in the trigeminal brainstem complex of the adult rat. J Comp Neurol 320:323-338.

Beul SF, Hilhetag CC. 2015. Towards a "canonical" agranular cortical microcircuit. Front Neuroanat doi: 10.3389/fnana.2014.00165

Bicanic I, Hladnik A, Petanjek Z. 2017. A quantitative Golgi study of dendritic morphology in the mice striatal medium spiny neurons. Front Neuroanat 11 37.

Braak H, Braak E.1982. Neuronal types in the claustrum of man. Anat Embryol 163:447–460.

Brand S. 1981. A serial section Golgi analysis of the primate claustrum. Anat Embryol 162:475–488.

Butti C, Janeway CM, Townshend C, Wicinski BA, Reidenberg JS, Ridgway SH, Sherwood CC, Hof PR, Jacobs B. 2015. The neocortex of cetartiodactyls: I. A comparative Golgi analysis of neuronal morphology in the bottlenose dolphin (*Tursiops truncatus*), the minke whale (*Balaenoptera acutorostrata*), and the humpback whale (*Megaptera novaeangliae*). Brain Struct Funct 220:3339–3368.

Cozzi B, Roncon G, Granato A, Giurisato M, Castagna M, Peruffo A, Panin M, Ballarin C, Montelli S, Pirone A. 2014. The claustrum of the bottlenose dolphin *Tursiops truncatus* (Montagu 1821). Front Syst Neurosci 8, 42.

Cozzi B, De Giorgio A, Peruffo A, Montelli S, Panin M, Bombardi C, Grandis A, Pirone A, Zambenedetti P, Corain L, Granato A. 2017. The laminar organization of the motor cortex in monodactylous mammals: a comparative assessment based on horse, chimpanzee, and macaque. Brain Struct Funct 222: 2743-2757.

Crick FC, Koch C. 2005. What is the function of the claustrum? Philos T R Soc B 360:1271–1279.

Day-Brown JD, Slusarczyk AS, Zhou N, Quiggins R, Petry HM, Bickford ME. 2016. Synaptic organization of striate cortex projections in the tree shrew: a comparison of the claustrum and dorsal thalamus. J Comp Neurol 52:1403–1420.

Deutch AY, Mathur BN. 2015. Editorial: the claustrum: charting a way forward for the brain's most mysterious nucleus. Front Syst Neurosci 9, 103.

Di Rocco F, Giannetti S, Gaglini P, Di Rocco C, Granato A. 2001. Dendritic Anomalies in a Freezing Model of Microgyria: A Parametric Study. Pediatr Neurosurg 34:57–62.

Di Rocco F, Giannetti S, Gaglini P, Di Rocco C, Granato A. 2002. Dendritic architecture of corticothalamic neurons in a rat model of microgyria. Childs Nerv Syst 18:690–693.

Druga R, Chen S, Bentivoglio M. 1993. Parvalbumin and calbindin in the rat claustrum: an immunocytochemical study combined with retrograde tracing frontoparietal cortex. J Chem Neuroanat 6:399–406.

Edelstein LR, Denaro FJ. 2004. The claustrum: a historical review of its anatomy, physiology, cytochemistry and functional significance. Cell Mol Biol 50:675–702.

Elston GN, Benavides-Piccione R, DeFelipe J. 2001. The pyramidal cell in cognition: a comparative study in human and monkey. J Neurosci 21 RC163.

Félix B, Léger ME, Albe-Fessard D, Marcilloux JC, Rampin O, Laplace JP, Duclos A, Fort F, Gougis S, Costa M, Duclos N. 1999. Stereotaxic atlas of the pig brain. Brain Res Bull 49:1–137.

Gerfen CR, Baimbridget KG, Miller JJ. 1985. The neostriatal mosaic: Compartmental distribution of calcium-binding protein and parvalbumin in the basalganglia of the rat and monkey. Proc Natl Acad Sci USA 82:8780-8784.

Giannetti S, Gaglini P, Di Rocco F, Di Rocco C, Granato A. 2000. Organization of cortico-cortical associative projections in a rat model of microgyria. NeuroReport 11:2185-2189.

Glezer II, Hof PR, Istomin VV, Morgane, PJ. 1995. Comparative immunocytochemistry of calcium-binding protein-positive neurons in visual and auditory systems of cetacean and primate brains. In Kastelein RA, Thomas JA, Nachtigall PE, editors. Sensory systems of aquatic mammals. De Spil Publishers, Woerden, The Netherlands. p 477-513.

Glezer II, Hof PR, Leranth C, Morgane, PJ. 1993. Calcium-binding protein-containing neuronal populations in mammalian visual cortex: a comparative study in whales, insectivores, bats, rodents, and primates. Cereb Cortex 3:249-272.

Glezer II, Hof PR, Morgane PJ. 1998. Comparative analysis of calcium-binding protein-immunoreactive neuronal populations in the auditory and visual systems of the bottlenose dolphin (*Tursiops truncatus*) and the macaque monkey (*Macaca fascicularis*). J Chem Neuroanat 15:203-237.

Godlove DC, Maier A, Woodman GF, Schall JD. 2014. Microcircuitry of agranular frontal cortex: testing the generality of the canonical cortical microcircuit. J. Neurosci 34: 5355-5369.

Goll Y, Atlan G, Citri A. 2015. Attention: the claustrum. Trends Neurosci 38:486–495.

Granato A, Di Rocco F, Zumbo A, Toesca A, Giannetti S. 2003. Organization of cortico-cortical associative projections in rats exposed to ethanol during early postnatal life. Brain Res Bull 60:339–344.

Hamilton DJ, Shepherd GM, Martone ME, Ascoli GA. 2012. An ontological approach to describing neurons and their relationships. Front Neuroinform 6, 15.

Hinova-Palova DV, Edelstein L, Landzhov BV, Braak E, Malinova LG, Minkov M, Paloff A, Ovtscharoff W. 2014. Parvalbumin- immunoreactive neurons in the human CL. Brain Struct Funct 219:1813–1830.

Hinova-Palova DV, Edelstein LR, Paloff AM, Hristov S, Papantchev VG, Ovtscharoff WA. 2007. Parvalbumin in the cat claustrum: ultrastructure, distribution and functional implications. Acta Histochem 109:61–77.

Hof PR, Glezer II, Condé F, Flagg, RA, Rubin MB, Nimchinsky EA, Vogt Weisenhorn DM. 1999. Cellular distribution of the calcium-binding proteins parvalbumin, calbindin, and calretinin in the neocortex of mammals: phylogenetic and developmental patterns. J Chem Neuroanat 16:77-116.

Hof PR, Glezer II, Nimchinsky EA, Erwin JM. 2000. Neurochemical and cellular specializations in the mammalian neocortex reflect phylogenetic relationships: evidence from primates, cetaceans, and artiodactyls. Brain Behav Evol 55:300-310.

Hu H, Gan J, Jonas P. 2014. Fast-spiking, parvalbumin+ GABAergic interneurons: From cellular design to microcircuit function. Science 345, 1255263.

Jacobs B, Harland T, Kennedy D, Schall M, Wicinski B, Butti C, Hof PR, Sherwood CC, Manger PR. 2015. The neocortex of cetartiodactyls. II. Neuronal morphology of the visual and motor cortices in the giraffe (*Giraffa camelopardalis*). Brain Struct Funct 220:2851–2872.

Jacobs B, Lubs J, Hannan M, Anderson K, Butti C, Sherwood CC, Hof PR, Manger PR. 2011. Neuronal morphology in the African elephant (*Loxodonta africana*) neocortex. Brain Struct Funct 215:273–298.

Jacobs B, Schall M, Prather M, Kapler E, Driscoll L, Baca S, Jacobs J, Ford K, Wainwright M, Treml M. 2001. Regional Dendritic and Spine Variation in Human Cerebral Cortex: a Quantitative Golgi Study. Cerebral Cortex 11:558–571.

Jelsing J, Hay-Schmidt A, Dyrby T, Hemmingsen R, Uylings HB, Pakkenberg B. 2006. The prefrontal cortex in the Göttingen minipig brain defined by neural projection criteria and cytoarchitecture. Brain Res Bull 70:322–336.

Johnson CB, Schall M, Tennison ME, Garcia ME, Shea-Shumsky NB, Raghanti MA, Lewandowski AH, Bertelsen MF, Waller LC, Walsh T, Roberts GF, Hof PR, Sherwood CC, Manger PR, Jacobs B.

2016. Neocortical Neuronal Morphology in the Siberian Tiger (*Panthera tigris altaica*) and the Clouded Leopard (*Neofelis nebulosa*). J Comp Neurol 524:3641–3665.

Johnson JI, Fenske BA, Jaswa AS, Morris JA. 2014. Exploitation of puddles for breakthroughs in claustrum research. Front Syst Neurosci 8, 78.

Kim J, Matney CJ, Roth RH, Brown SP. 2016. Synaptic Organization of the Neuronal Circuits of the Claustrum. J Neurosci 36:773–784.

Kowianski P, Dziewiatkowski J, Kowianska J, Moryś J. 1999. Comparative anatomy of the claustrum in selected species: a morphometric analysis. Brain Behav Evol 53:44–54.

Kowianski P, Dziewiatkowski J, Moryś JM, Majak K, Wójcik S, Edelstein LR, Lietzau G, Moryś J. 2009. Colocalizationof neuropeptides with calcium-binding proteins in the claustral interneurons during postnatal development of the rat. Brain Res Bull 80:100–106.

LeVay S, Sherk H. 1981. The visual claustrum of the cat. I. Structure and connections. J Neurosci 1:956–980.

Lind NM, Moustgaard A, Jelsing J, Vajta G, Cumming P, Hansen AK. 2007. The use of pigs in neuroscience: modeling brain disorders. Neurosci Biobehav Rev 31:728–751.

Mainen ZF, Sejnowski TJ. 1996. Influence of dendritic structure on firing pattern in model neocortical neurons. Nature 382:363-366.

Mathur BN. 2014. The claustrum in review. Front Syst Neurosci 8, 48.

Mathur BN, Caprioli RM, Deutch AY. 2009. Proteomic Analysis Illuminates a Novel Structural Definition of the Claustrum and Insula. Cerebral Cortex 19:2372-2379.

Orman R, Kollmar R, Stewart M. 2017. Claustrum of the short-tailed fruit bat, *Carollia perspicillata*: alignment of cellular orientation and functional connectivity. J Comp Neurol 1474: 1459–1474.

Pirone A, Cantile C, Miragliotta V, Lenzi C, Giannessi E, Cozzi B. 2016. Immunohistochemical distribution of the cannabinoid receptor 1 and fatty acid amide hydrolase in the dog claustrum. J Chem Neuroanat 74:21–27.

Pirone A, Castagna M, Granato A, Peruffo A, Quilici F, Cavicchioli L, Piano I, Lenzi C, Cozzi B. 2014. Expression of calcium-binding proteins and selected neuropeptides in the human, chimpanzee, and crab-eating macaque claustrum. Front Syst Neurosci 8, 99.

Pirone A, Cozzi B, Edelstein L, Lenzi C, Quilici F, Antonini R, Castagna M. 2012. Topography of Gng2- and NetrinG2-expression suggests an insular origin of the human claustrum. PLoS ONE 7(9) e44745.

Pirone A, Magliaro C, Giannessi E, Ahluwalia A. 2015. Parvalbumin expression in the claustrum of the adult dog. An immunohistochemical and topographical study with comparative notes on the structure of the nucleus. J Chem Neuroanat 64–65:33–42.

Pirone A, Miragliotta V, Ciregia F, Giannessi E, Cozzi B. 2018. The catecholaminergic innervation of the claustrum of the pig. J Anat 232:158-166.

Rahman FE, Baizer JS. 2007. Neurochemically defined cell types in the claustrum of the cat. Brain Res 1159:94–111.

Rausell E, Bae CS, Viñuela A, Huntley GW, Jones EG. 1992. Calbindin and Parvalbumin cells in monkey VPL thalamic nucleus: distribution, laminar cortical projections, and relations to spinothalamic terminations. J Neurosci 12:4088-4111.

Rees CL, Moradi K, Ascoli GA. 2017. Weighing the evidence in Peters' rule: does neuronal morphology predict connectivity? Trends Neurosci 40:63–71.

Reser DH, Majka P, Snell S, Chan JM, Watkins K, Worthy K, Quiroga MD, Rosa MG. 2017. Topography of claustrum and insula projections to medial prefrontal and anterior cingulate cortex of the common marmoset (*Callithrix jacchus*). J Comp Neurol 525:1421–1441.

Reynhout K, Baizer JS. 1999. Immunoreactivity for calcium-binding Proteins in the claustrum of the monkey. Anat Embryol 199:75–83.

Saparov A, Schwemmer MA 2015. Effects of passive dendritic tree properties on the firing dynamics of a leaky-integrate-and-fire neuron. Math Biosci 269: 61-75.

Shankaranarayana Rao BS, Raju RT. 2004. The Golgi techniques for staining neurons. In: Raju RT, Kutty BM, Sathyaprabha TN, Shankaranarayana Rao BS, editors. Brain and behavior. Bangalore, India: NIMH and Neuro Sciences. p 108–11.

van Kann E, Cozzi B, Hof PR, Oelschläger HHA. 2017. Qualitative and quantitative analysis of primary neocortical areas in selected mammals. Brain Behav Evol 90:193-210.

van Ooyen A, Duijnhouwer J, Remme MW, van Pelt J. 2002. The effect of dendritic topology on firing patterns in model neurons. Networks 13:311-325.

Wang Q, Ng L, Harris JA, Feng D, Li Y, Royall JJ, Oh SW, Bernard A, Sunkin SM, Koch C, Zeng H. 2017. Organization of the connections between claustrum and cortex in the mouse. J Comp Neurol 1346:1317–1346.

Watakabe A. 2017. In situ hybridization analyses of claustrum-enriched genes in marmosets. J Comp Neurol 525:1442–1458.

Watson C, Puelles L. 2017. Developmental gene expression in the mouse clarifies the organization of the claustrum and related endopiriform nuclei. J Comp Neurol 525:1499–1508.

Watson GDR, Smith JB, Alloway KD. 2017. Interhemispheric Connections Between the Infralimbic and Entorhinal Cortices: The Endopiriform Nucleus Has Limbic Connections That Parallel the Sensory and Motor Connections of the Claustrum. J Comp Neurol 525:1363–1380.

White MG, Panicker M, Mu C, Carter AM, Roberts BM, Dharmasri PA, Mathur BN. 2018. Anterior Cingulate Cortex Input to the Claustrum Is Required for Top-Down Action Control. Cell Reports 22:84–95.

Zaqout S, Kaindl AM. 2016. Golgi-Cox Staining Step by Step. Front Neuroanat 10, 18.

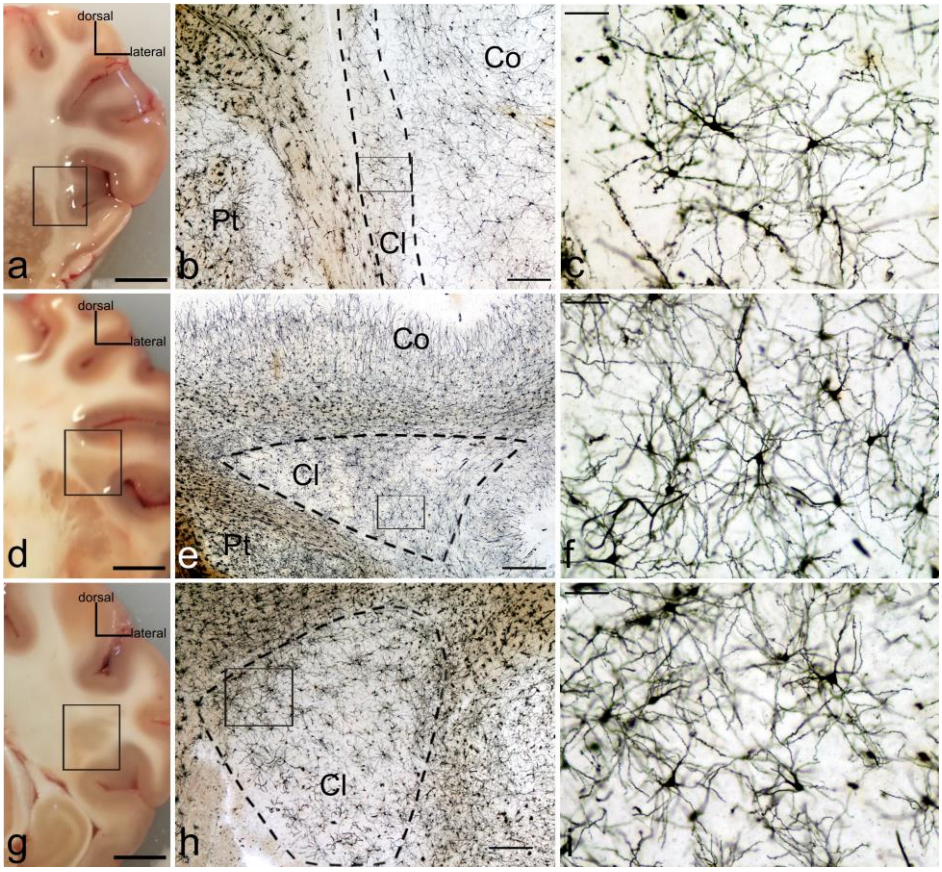

Figure 1. Golgi-Cox staining of the selected brain blocks. Left column (a, rostral; d, middle; g, caudal): photographs of coronal sections of fresh pig brain showing the claustrum (black frames). b, e, h: Golgi-Cox stained claustrum (Cl) and adjoining structures (Co, cortex; Pt, putamen) corresponding to the frames in the left column. c, f, i: higher magnification of the zone indicated with the black frames in b, e, h showing stained neurons in the claustrum. Right column, drawings showing the shape of the claustrum (red line) at different rostro-caudal levels. Scale bars = 0,5 cm (a, d, g); 500 µm (b, e, h); 100 µm (c, f, i).

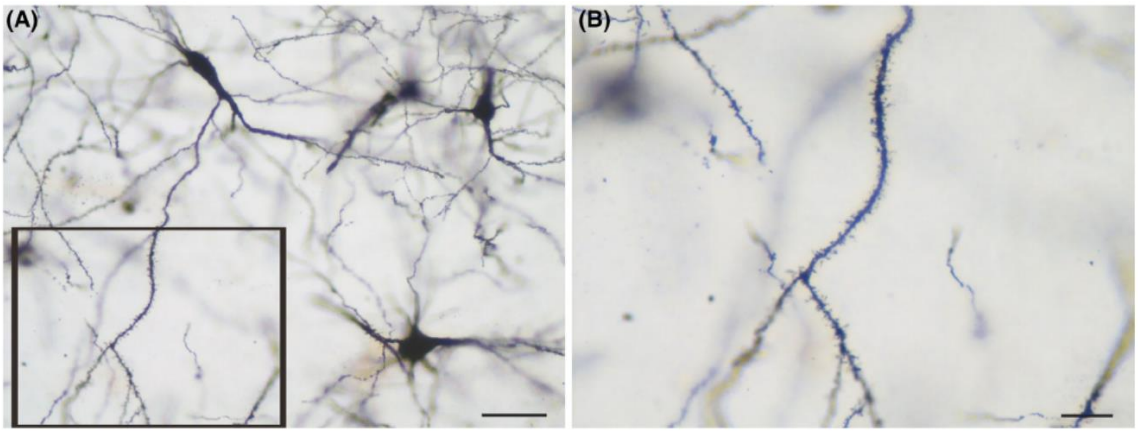

Figure 2. (a) Golgi-Cox stained neurons of the pig claustrum with fully impregnated soma and completed dendritic arbors. (b) Higher magnification of image a displaying the presence of spines on a dendrite. Scale bars = 50 µm (a); 20 µm (b).

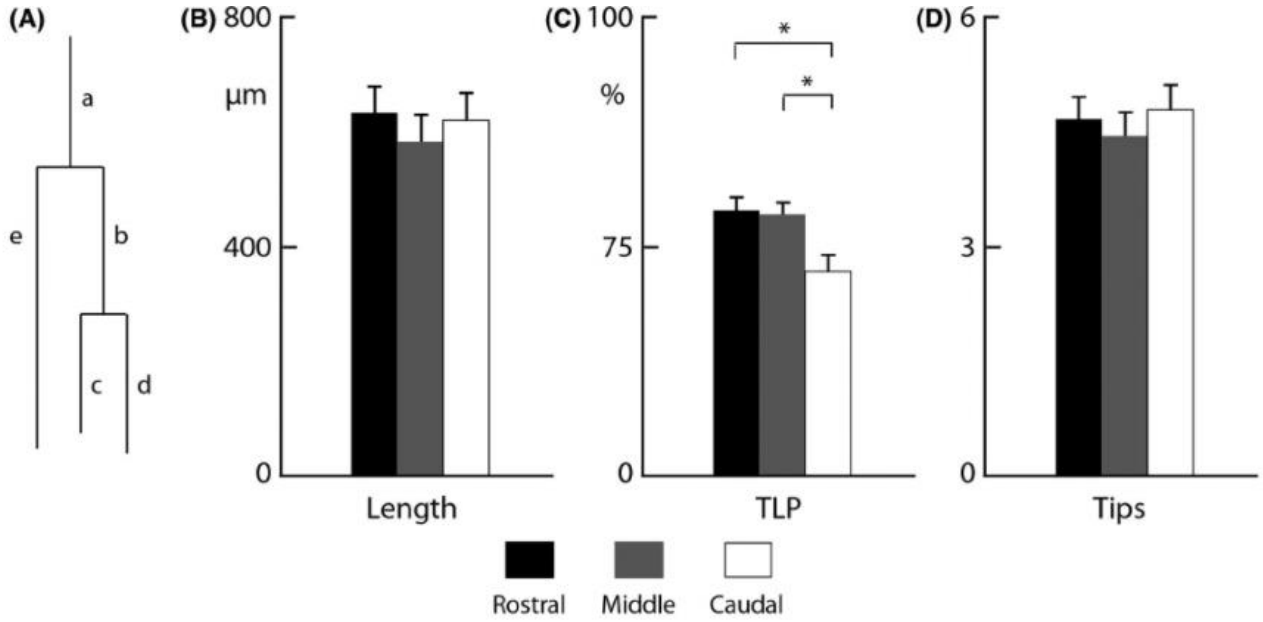

Figure 3. Quantitative parameters obtained after 3D reconstruction of claustral neuron dendrites. All data are expressed as mean (bars) ± standard error of the mean (T-bars). For each parameter, data from rostral, middle, and caudal claustral sections are shown. A. Dendrogram showing the method used for the computation of quantitative parameters. Total dendritic length = a + b + c + d + e. Terminal length percentage (i.e. the percentage of the total length occupied by the terminal branches) = 100 [(c + d + e) / (a + b + c + d + e)]. The number of terminal tips for this representative dendrite is 3. B. total dendritic length. C. terminal length percentage (TLP). D. number of terminal dendritic tips. *: $P < 0.05$.

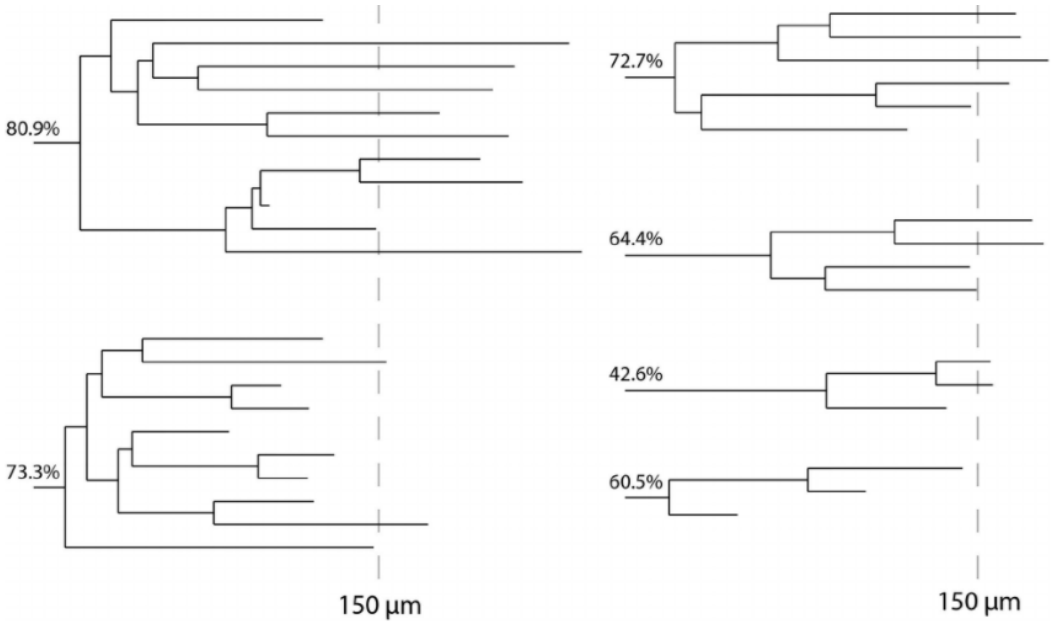

602

603 **Figure 4.** Dendrograms showing the six dendrites of a neuron from the caudal section of the
604 claustrum. The length of the branches is represented only on the horizontal lines. Vertical lines
605 represent branching points and do not express metric properties. The terminal length percentage of
606 each dendrite is also reported.

607

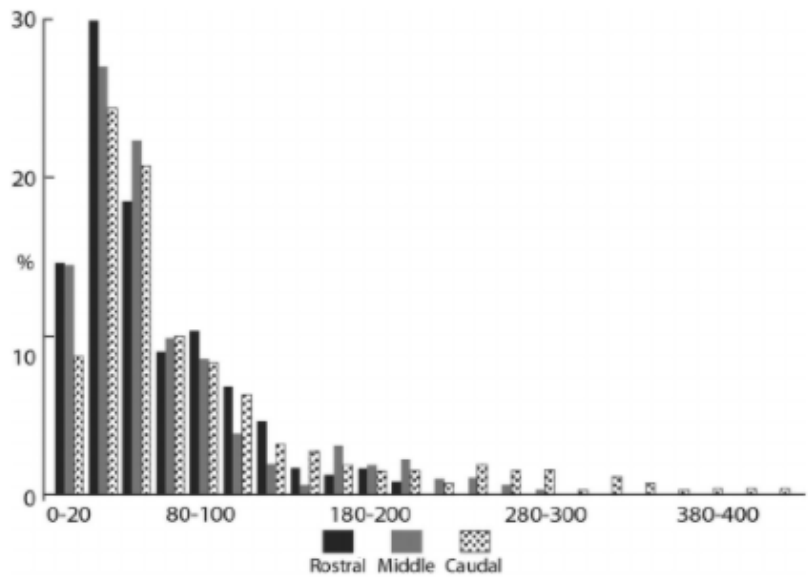

608

609 **Figure 5**. Sholl analysis showing the percent distribution of branching nodes plotted against the
610 distance from the soma. Bins (intervals of the circle radius) are 20 µm.

611

612

613

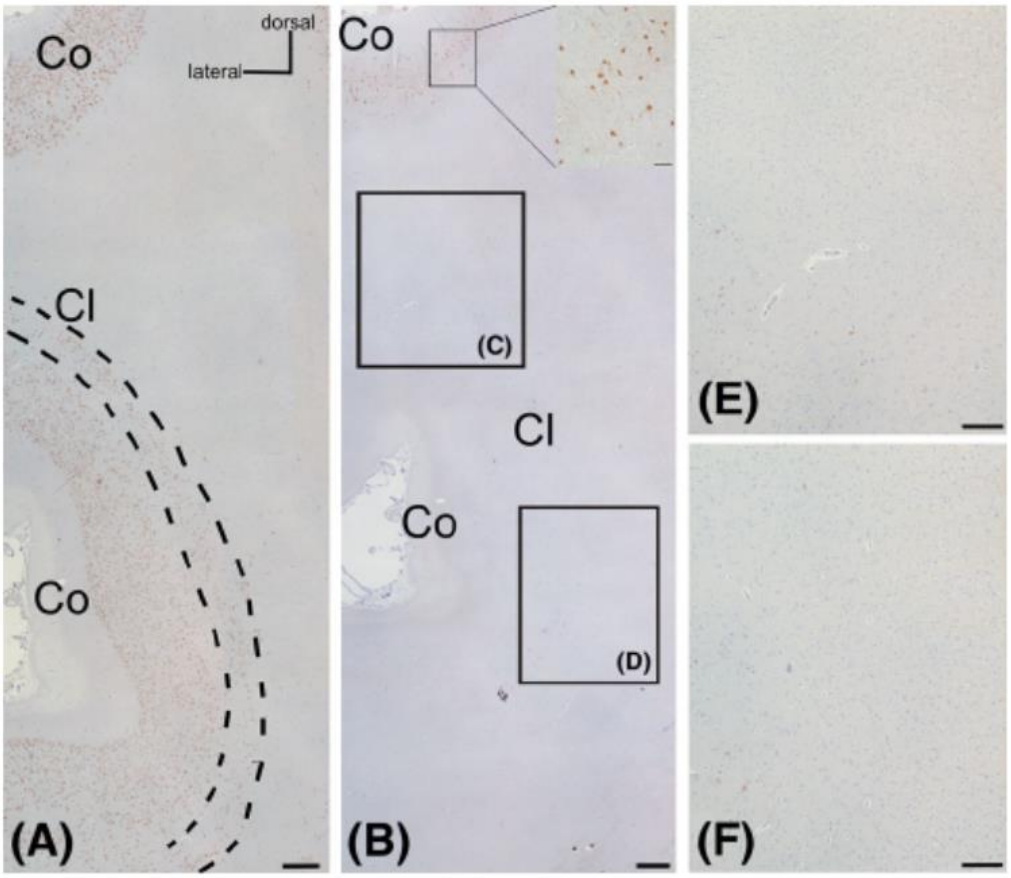

Figure 6. Immunohistochemical staining of the anterior claustrum. (a) NeuN-immunoreactive neurons in the cortex (Co) and in the claustrum (Cl, dashed line). (b) PV immunolabeling showing the presence of immunoreactive neurons (inset) in the dorsal cortex (Co) and the absence of PV positive neurons in the claustrum (Cl, frames c and d) and in the adjacent cortex. (e) and (f) represent respectively higher magnifications of the frames c and d of the image b. Scale bars = 500 µm (a, b); 200 µm (e, f); 100 µm (inset).

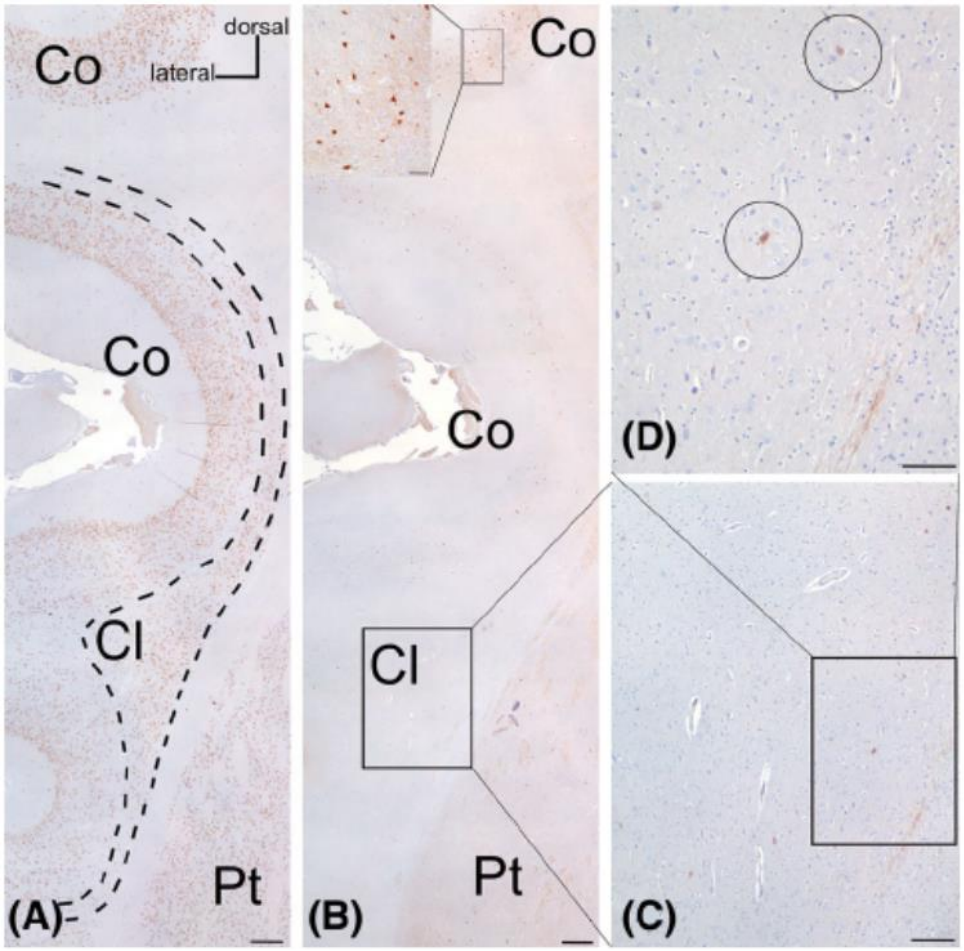

Figure 7. Immunohistochemical staining of the middle claustrum. (a) NeuN-immunoreactive neurons in the cortex (Co) and in the claustrum (Cl, dashed line). (b) PV immunolabeling showing the presence of immunoreactive neurons (inset) in the dorsal cortex (Co) and very scarce positive neurons in the claustrum (circles figure d). (c) higher magnification of the frame in figure b. (d) higher magnification of the frame in figure c.. Scale bars = 500 μm (a, b); 200 μm (c); 100 μm (d, inset).

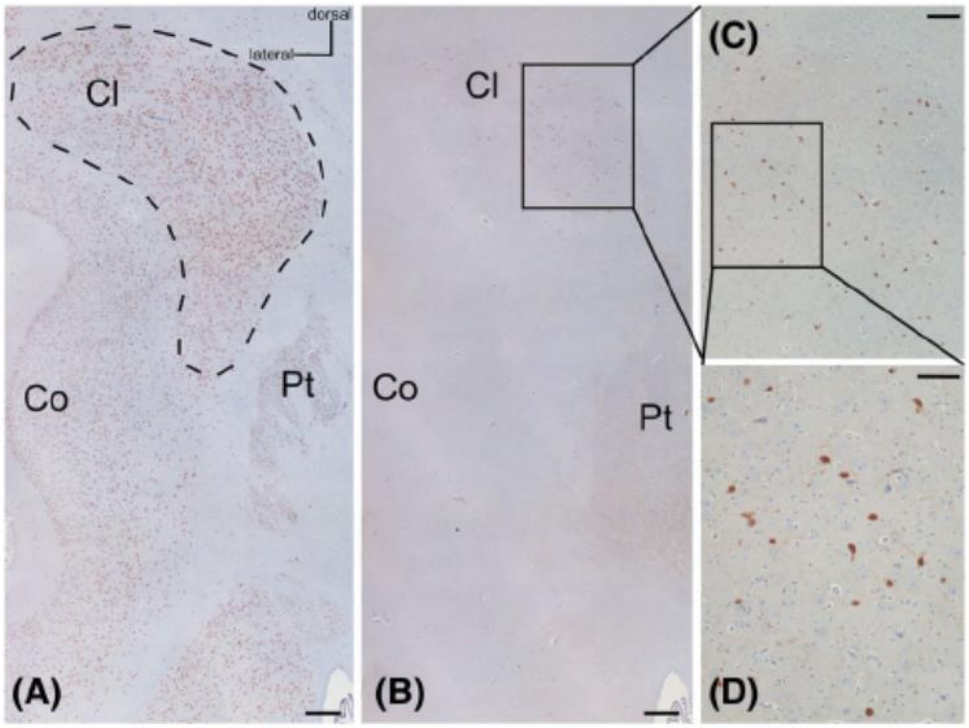

Figure 8. Immunohistochemical staining of the posterior claustrum. (a) NeuN labeling identifies the large posterior puddle of the claustrum (Cl, dashed line). (b) Immunoperoxidase reaction shows the presence of PV-immunoreactive neurons in the claustrum (black frame). (c) higher magnification of the frame in figure b. (d) higher magnification of the frame in figure c. Scale bars = 500 µm (a, b); 200 µm (c); 100 µm (d).